SoRo
Soft Robotics

ORIGINAL ARTICLE

Toward Modular Soft Robotics: Proprioceptive Curvature Sensing and Sliding-Mode Control of Soft Bidirectional Bending Modules

Ming Luo, Erik H. Skorina, Weijia Tao, Fuchen Chen, Selim Ozel, Yinan Sun, and Cagdas D. Onal

Abstract

Real-world environments are complex, unstructured, and often fragile. Soft robotics offers a solution for robots to safely interact with the environment and human coworkers, but suffers from a host of challenges in sensing and control of continuously deformable bodies. To overcome these challenges, this article considers a modular soft robotic architecture that offers proprioceptive sensing of pressure-operated bending actuation modules. We present integrated custom magnetic curvature sensors embedded in the neutral axis of bidirectional bending actuators. We describe our recent advances in the design and fabrication of these modules to improve the reliability of proprioceptive curvature feedback over our prior work. In particular, we study the effect of dimensional parameters on improving the linearity of curvature measurements. In addition, we present a sliding-mode controller formulation that drives the binary solenoid valve states directly, giving the control system the ability to hold the actuator steady without continuous pressurization and depressurization. In comparison to other methods, this control approach does not rely on pulse width modulation and hence offers superior dynamic performance (i.e., faster response rates). Our experimental results indicate that the proposed soft robotic modules offer a large range of bending angles with monotonic and more linear embedded curvature measurements, and that the direct sliding-mode control system exhibits improved bandwidth and a notable reduction in binary valve actuation operations compared to our earlier iterative sliding-mode controller.

Keywords: proprioceptive, sliding mode, curvature control, integrated, soft bidirectional bending actuator, standardized design and fabrication, module

Objectives

ADVANTAGES OF SOFT robotic systems over traditional robots include compliant adaptation to unstructured or unknown environments, organic bio-inspired mobility and manipulation, and increased safety for human robot collaboration.[1–4] Some examples of bio-inspired soft robotic systems are a caterpillar and star fish,[5–7] both of which require considerable flexibility, making rigid links unsuitable. Soft continuum robotic manipulators can operate in complex environments while being friendly for human–robot interaction.[8–12] The soft muscles used in soft robotic systems can have variable stiffness properties instead of the rigid DC motors,[13–15] allowing them to adapt to different tasks, such as surgery and rehabilitation.[16–18]

However, the emerging nature of the fluidic elastomer actuators used in recent soft robotic research presents challenges in reliable and repeatable operation based on standardized design and fabrication principles, integrated deformation sensing without sacrificing flexibility for proprioception, and feedback motion control in low bandwidth due to large response times of these soft actuation systems.

Our previous work focused on soft bidirectional bending actuators as segments in a soft kinematic chain toward a soft robotic snake or an octopus manipulator arm.[19–23] These segments comprise two pressure chambers on either side of an inextensible constraint layer. When one chamber is pressurized, geometric constraints cause it to extend in the axial direction, but the segment as a whole is prevented from

WPI Soft Robotics Lab, Mechanical Engineering Department, Robotics Engineering Program, Worcester Polytechnic Institute, Worcester, Massachusetts.

FIG. 1. CAD model (*left*) and experimental prototype (*right*) of the proposed soft bidirectional bending actuator module with integrated curvature sensing.
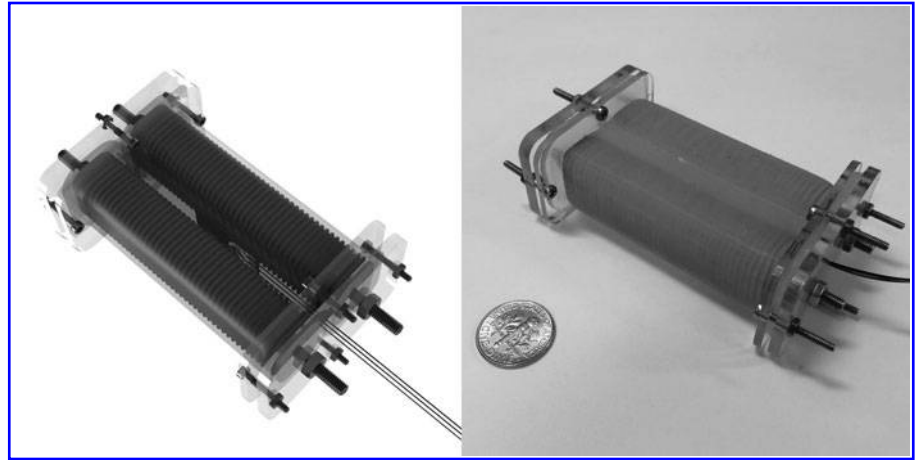
extending by the central constraint layer. Thus, the entire segment bends away from the pressurized chamber.[22]

Using soft actuation segments for practical robotic applications necessitates a method of measuring their state. To this end, various sensors have been developed, including an optical fiber Bragg grating sensor used for measuring forces[24,25] and shape reconstruction.[26] In addition, eutectic gallium–indium (eGaIn) has been embedded in silicone rubber and used to measure curvature[27,28] and forces[29] through changes in resistance. In our prior work, we developed a magnetic curvature sensor using a composite multilayer molding process compatible with soft robotic fabrication methods,[30] which offers fast response and repeatable operation without hysteresis.

The latest generation of our soft bidirectional bending actuators utilizes two acrylic plates and a vent screw as fluidic end connectors to improve operational reliability, and integrates our magnetic curvature sensor in the constraint layer (neutral axis). However, the fabrication process of these actuators is complicated, because three pieces need to be bonded together: two end connectors and the body, which also presents a point of failure under large pressure inputs. In addition, the curvature sensor on the middle constraint layer of this design can often be disrupted by the expanding pressure chambers. This was evidenced by nonmonotonic bumps and nonlinearities in the sensor data in our earlier work.[23]

Control in the context of soft robotics has very little precedence, emphasizing the complexity in devising motion control algorithms for these inherently slow response systems. Work was done controlling a unidirectional soft pneumatic bending segment using fiber Bragg grating for sensing and valve pulse width modulation (PWM) for actuation, but with a slow response time.[31]

In our previous work, we focused on an iterative sliding-mode controller (iterative SMC) augmented by a feedforward term on a simple 1 degree of freedom (DoF) revolute joint operated antagonistically by two linear soft pneumatic actuators we call reverse pneumatic artificial muscles.[32] The iterative SMC utilized PWM of miniature solenoid valves as an approximation of analog pressure control. We recently adapted this control approach to our soft bidirectional bending actuator to compare our custom magnetic curvature sensor[22] with an off-the-shelf flex sensor, whose resistive sensing modality suffers from significant dynamic artifacts.[21] Our results indicate that despite its utility in feedback motion control of soft robots, this controller requires solenoid valves

to be continuously switched on and off reducing their operational lifetime, and forces the feedback control loop to run at a relatively low frequency due to PWM discretization.

This article debuts our fourth-generation soft bidirectional bending actuator, shown in Figure 1. The fundamental benefit
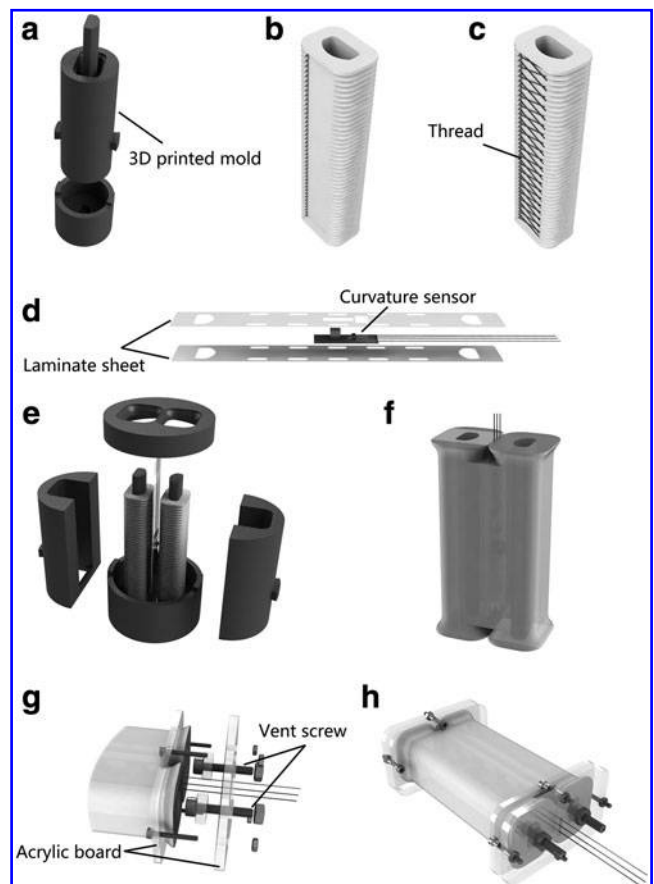
FIG. 2. Fabrication process of the soft actuator. **(a)** The mold of a single actuator. **(b)** The single linear actuator without thread. **(c)** The single linear actuator. **(d)** The constraint layer with the curvature sensor and two laminate sheets. **(e)** The mold used to combine the two linear actuators with the constraint layer. **(f)** The demolded soft actuator. **(g)** The connector includes the acrylic board and the vent screw. **(h)** The final version of the soft bending actuator.

of the proposed actuator is it does not require bonding separate pieces of silicone rubber together to form the pressure chambers and instead focuses on a standardized design and fabrication approach that eliminate bonding for stronger and more repeatable soft bending actuation modules.

We seek to solve the sensor nonlinearity problem,[23] discussed in more detail later, by testing two different chamber cross sections of this new actuator: rectangular and semicircular (with the circular side facing inward). We also seek to increase the bandwidth of the feedback control loop by using a more complicated valving scheme alongside a sliding-mode controller directly regulating valve states (direct SMC). This method allows the system to hold pressure in the actuator, reducing the chattering in the valves and increasing their life span.

The objectives of this work include the following:

- To effectively integrate curvature sensing and soft bending actuation.
- To standardize and simplify the design and fabrication of soft bidirectional bending actuation modules.
- To demonstrate advances in motion control of pneumatic soft actuators.

Materials and Methods

Soft bending actuation modules

Our soft bending actuator comprises two soft linear muscles and an inextensible constraint layer in between. The individual linear actuators are made of tubes of silicone rubber wrapped in inextensible thread, which causes them to extend with reduced radial deformation when pressurized. The constraint

layer, with a custom integrated curvature sensor, inhibits this linear extension, resulting in the bending of the entire soft module. Caps are attached to both ends of the actuator to seal the chambers and allow for connection with other segments. The caps are made of two acrylic boards sandwiching the rim of the silicone rubber tube to prevent leaking.

Thus, the silicone rubber substrate itself is used as a gasket, eliminating the need for airtight bonds between separate pieces of silicone, a major failure point in the past. Screws are used at either end to allow for easy mounting, with one side using vent screws to allow pressure to be introduced into the chamber. The rectangular external cross section of the actuators reduces potential twisting that occurs at high bending angles and pressure inputs. The steps of fabrication can be summarized as follows (Fig. 2):

Step 1: Two inner bodies (i.e., linear muscles) of the module are fabricated first using a three-dimensional (3D) printed mold and silicone rubber (Smooth-On Ecoflex 0030).

Step 2: Inextensible sewing thread is wrapped and bonded around each linear muscle.

Step 3: With the flexible curvature sensor in the middle, two pieces of self-adhesive laminate sheet are laser cut and attached together to form the constraint layer.

Step 4: The constraint layer and two inner bodies are placed in a second 3D printed mold and filled with silicone rubber.

Step 5: Acrylic end-connector caps and vent screws are attached to both ends of the body.

Proprioceptive curvature sensing

Our custom magnetic curvature sensor was initially developed in the previous work,[30] which utilized a magnet and a
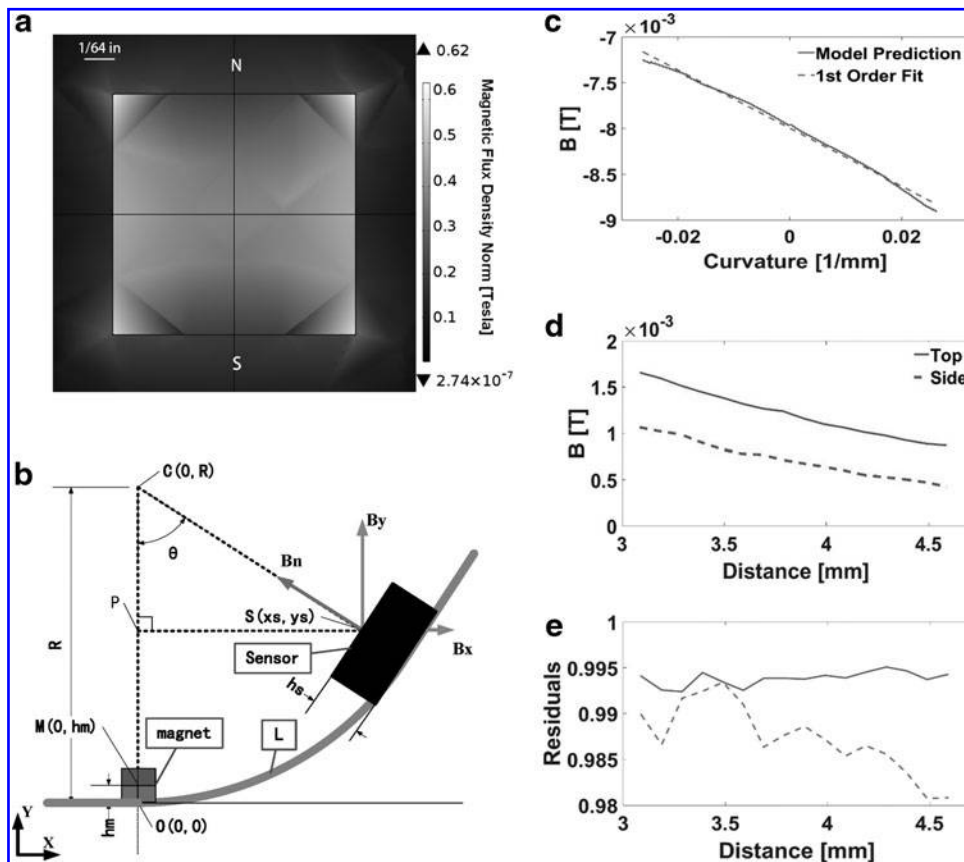
FIG. 3. Finite element analysis of the flexible curvature senor. **(a)** A two-dimensional view of magnetic field vectors from our COMSOL simulation. **(b)** The geometric relationship between the magnet and the Hall effect sensor. **(c)** The simulated magnetic field data at the sensor (*solid line*) and a corresponding first-order fit (*dashed line*) as a function of curvature. The magnet is facing out of the sensor (the N direction is upward) and the distance L is 3.1 mm. **(d)** The effect of changing L and magnet orientation on measured magnetic field at a 90° bending angle. The *solid line* shows the data where the magnet is facing upward (y-axis) and the *dashed line* shows the magnet facing sideways (x-axis, i.e., toward the Hall effect sensor). **(e)** The residuals of linear fits on data from **(d)** representing the linearity of the data.

one-dimensional Hall effect sensor on a flexible circuit board. The Hall effect sensor can measure changes in the magnetic field as the sensor bends, allowing us to accurately calculate the curvature of the system. We revised the circuit design in the previous work,[21,22] making the magnetic north of the magnet point out of the circuit surface. In this configuration, we could adjust the signal offset at zero curvature by manually changing the distance between the magnet and the Hall element. This method was very fragile because the traces required for the amplification circuit were prone to breaking as the sensor flexed. The circuit contained three layers: two laminate polyester sheets and one copper layer. The melting point of the laminate sheet is very low, which causes difficulties in soldering.

To address these problems, we removed the amplification circuit from the flexible sensor,[23] utilized a smaller Hall element, and constructed the sensor out of a single layer of copper-clad flexible polyimide substrate (Pyralux; 3M). This section builds on this body of work to develop custom magnetic curvature sensors that provide reliable proprioceptive information when integrated in soft bending actuators.

We used finite element analysis (FEA) to improve the design of our curvature sensor. We considered two main parameters: the orientation of the magnet and the distance between the magnet and the Hall element. First, we generated magnetic field data using COMSOL, an example of which can be seen in Figure 3a. We used this to calculate the strength of the magnetic field at the Hall element with respect to the circuit design. Figure 3b shows the geometric relationship between the magnet and the Hall element on a bending segment. The origin is located at the base of the magnet, L is the arc-length along the flexible circuit between the origin and the center of the Hall element, h_m is the height of the center of the magnet (point M), and h_s is the height of the Hall effect sensor element (point S). We assume that the flexible sensor is under constant curvature, allowing us to calculate the positions of these two points.

We can calculate the vector between M and S, and then use the COMSOL magnetic field data B_x and B_y at S to determine the expected field registered by the Hall element (in its normal direction) via the following rotation equation:

$$B_n = B_y cos\theta - B_x sin\theta. \tag{1}$$

where B_n is the magnetic field density, which the one-dimensional Hall effect sensor could sense when the bending angle is θ.

When analyzing the sensor simulation, we considered the working range of the bending actuator to be $\pm90°$, representing the bounds of θ. Figure 3c shows the model prediction of the magnetic field with respect to curvature at a distance of $L = 3.1$ mm, the results of which can be approximated using a linear fit. To determine the optimal distance and magnet orientation, we calculated the range of measured magnetic fields for L ranging between 3.1 and 4.6 mm with the magnetic north pointing upward (along y-axis) and sideways (along x-axis), the results of which can be seen in Figure 3d. This range was chosen to keep the sensor from coming into contact with the magnet at larger curvature values, as well as keep the magnetic field from becoming too weak to be measured effectively.

These sensor readings can each be approximated by a linear fit, as in Figure 3c. We compared the residuals (R^2 values) for these fits for top- and side-facing magnets for

the same range of L, representing the linearity of the resulting data. The results of this analysis can be seen in Figure 3e. We conclude that the top-facing magnet orientation is superior, because the working range is 30% larger and the data are more linear. In addition, it is found to be advantageous to minimize L to maximize the range of magnetic field readings.

In previous work,[23] we found that the integrated curvature sensor response was nonmonotonic at low actuation pressures, as seen in Figure 4e. This behavior made parsing the sensor data difficult at low angles and caused inconsistencies in segment motion data. We postulate that silicone rubber on the inside edge of an actuator is deforming when pressurized and pressing against the sensor, causing anomalous readings, and that the cross section of the pressure chamber has a direct effect on this behavior (as pressure is introduced, we expect the rectangular chamber to deform into a circular cross section). An illustration of this behavior for unpressurized and pressurized states of a rectangular cross-section actuator can been seen in Figure 4a and c, respectively.

Thus, to prevent this effect, we modified the pressure chamber cross section to semicircular, which can be seen in Figure 4b with its pressurized form Figure 4d, where it does not deform the sensor. We used an external vision tracker to calculate ground truth segment curvatures corresponding to
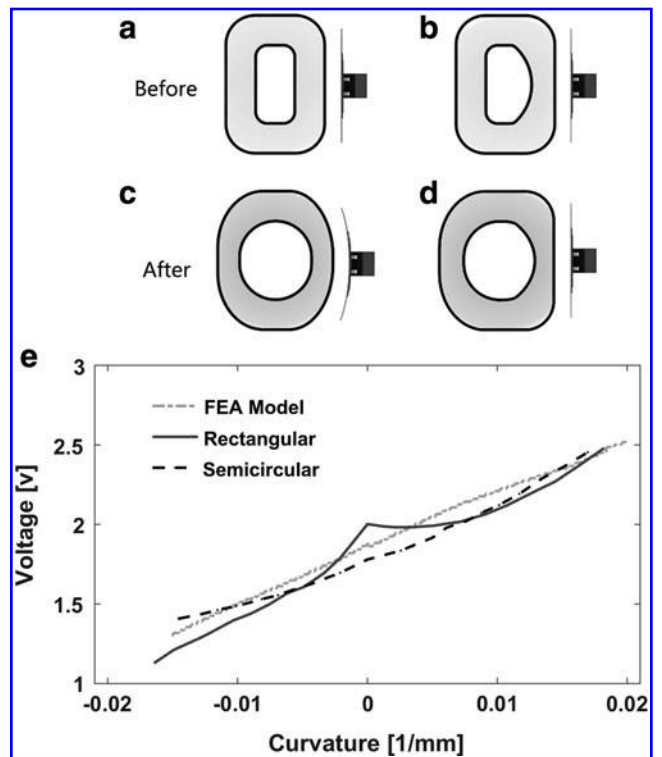
FIG. 4. The rectangular (**a**) and semicircular (**b**) shapes of the actuator pressure chamber cross section deform into circular shapes on pressurization in (**c**) and (**d**), respectively. Notice that the rectangular chamber in (**c**) deforms more against the sensor, causing it to bow. The sensor calibration data of the two chamber types in (**e**) indicate that the proposed semicircular cross section yields injective response. The rectangular chamber data are not monotonically increasing with bending curvature, making it inappropriate for feedback around small curvature values. The *solid line* is the FEA model prediction. FEA, finite element analysis.
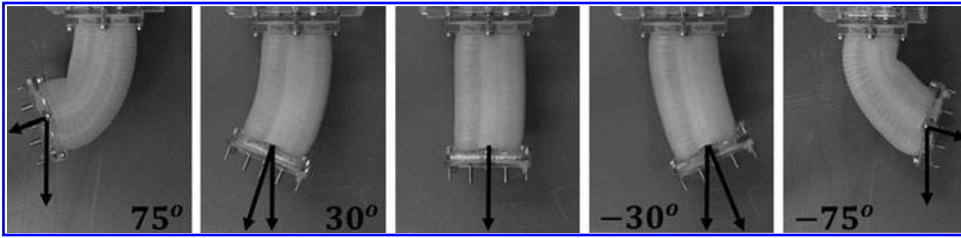
FIG. 5. Static response of the bending soft robotic module in a range of 150° at ±11 psi.

the recorded sensor voltages. Figure 4e shows these calibration curves for the two different chamber cross sections.

In addition, we also converted the numerical magnetic flux data to sensor voltage based on the sensitivity of the Hall effect sensor and the amplification circuit parameters. Again, we observed that the rectangular chamber data are not monotonic at small curvatures, meaning that the sensor is incapable of detecting changing angles at low-pressure inputs. The sensor readings with the semicircular cross section remain injective and more linear. In addition, the FEA model prediction fits these experimental data much better. This improvement makes the integrated curvature sensor more reliable, precise, and easier to use.

Sliding-mode motion control

In our previous work,[32] we used an iterative sliding-mode controller (iterative SMC) to control the pressure in each actuator. This was done using pulse width modulation; opening and closing the valves of each actuator to alternately inflate and deflate each actuator at a certain duty cycle as control input. The valves each have a response time of 3 ms, are about $7 \times 12 \times 30$ mm, and each cost around \$30. This method changes the amount each actuator is pressurized with respect to the previous time step based on the error between the current angle and the desired angle, thus iteratively correcting for errors as follows:

$$u(t) = u(t - \Delta t) + K (\dot{e}_x + D e_x), \qquad (2)$$

where $u(t)$ is the current control input, $u(t–\Delta t)$ is the previous control input, e_x is the error, $\dot{e}_x$ is the derivative of error, and K and D are control coefficients with units of s/degree and 1/s respectively.

One problem of this control method is that it involves constantly inflating and deflating each pneumatic chamber, even when the desired angle is constant. This causes the bending actuator to continuously oscillate around its target and potentially reduces the lifetime of the miniature solenoid valves.

To improve on this, we have adapted our pneumatic circuit to have separate valves on the inlet and outlet of each actuator. This makes it possible for a constant pressure to be held within the chambers, keeping them steady. We derive a direct sliding-mode controller (direct SMC) with this valve setup, defining

$$\sigma(t) = \dot{e}_x + D e_x, \qquad (3)$$

where $\sigma(t)$ is the sliding-mode variable ($\sigma = 0$ describes the sliding manifold). We define three control states (modes). If $\sigma > \varepsilon$ (ε represents a dead zone around the target), the module is driven in one direction by venting one actuator and filling the

other. If $\sigma < -\varepsilon$, the module is driven in the opposite direction. However, if $-\varepsilon < \sigma < \varepsilon$, the controller holds the pressure in both actuators, keeping the module at a steady curvature.

Results

We first observed the static behavior of our bending module, snapshots of which can be seen in Figure 5. At 30° bending in both directions, we can see that the actuator bends smoothly and with constant curvature. The actuator is capable of bending up to 75° in both directions, although this large bending angle seems to result in a less smooth curved shape. This is smaller than the 90° bounds we used to model the sensors, as the pressures required to reach 90° can be dangerous to the actuator at prolonged periods. The unactuated side of the actuator is forced to compress so much at that angle that a crease forms, while the central constraint layer is observed to remain smooth. The actuator can reliably withstand pressures of 7 psi (48.3 kPa), which was the pressure used for all subsequent experiments.
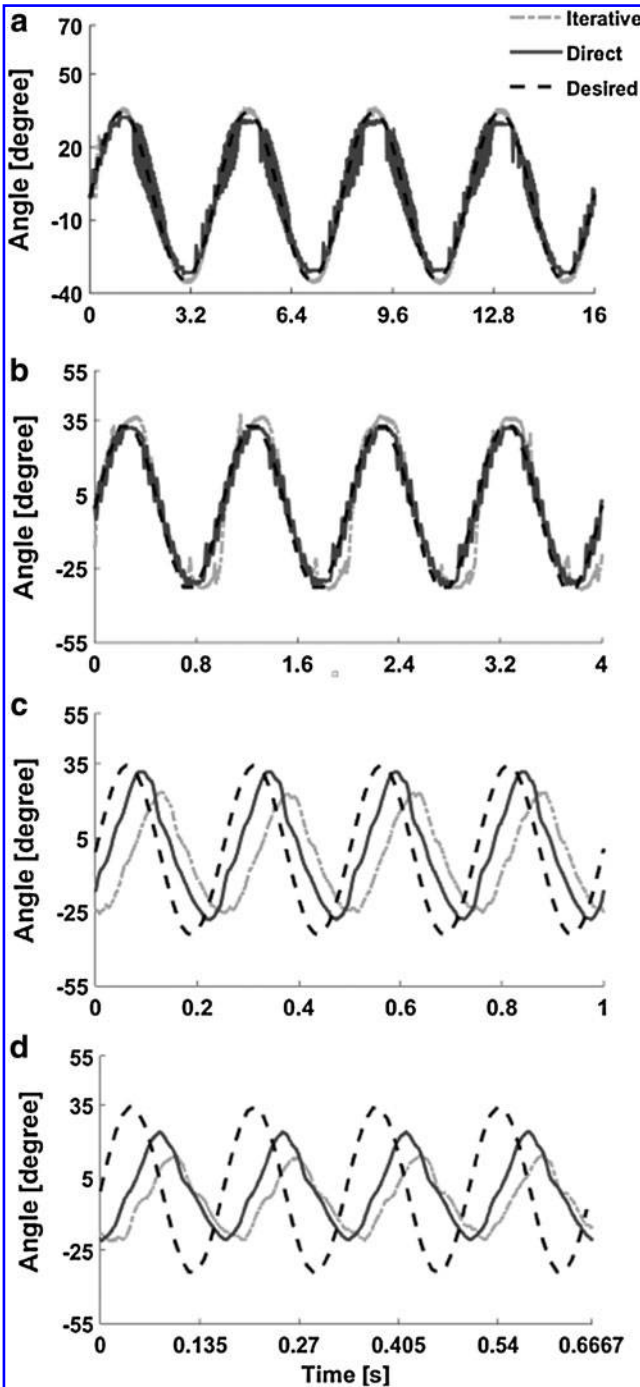
We tested both controllers on the integrated soft bending actuator for step and sinusoidal bending angle references. For the iterative SMC, we used $K = 1.5$ s/degree and $D = 0.0067$ 1/s. For the direct SMC, we used $D = 0.5$ 1/s and $\varepsilon = 2$ degree/s. These coefficients were tuned by hand to maximize performance, focusing on minimizing rise time and then limiting subsequent oscillations. Figure 6 shows the response of the controllers to a constant desired angle (step response). Unsurprisingly, the direct SMC exhibits far less oscillation at the
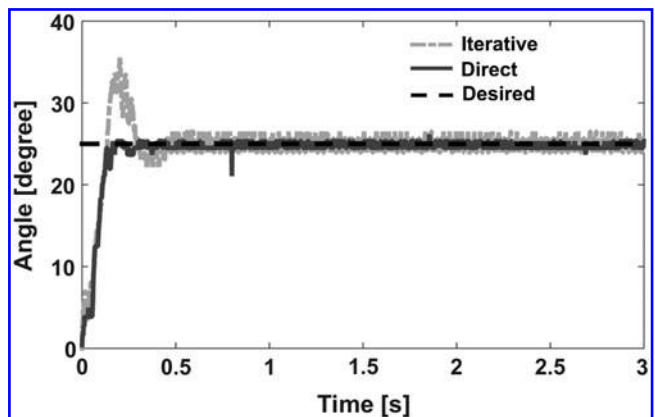
FIG. 6. Step response of the two controllers. The *dashed line* is the desired bending angle (25°) and the *light* and *dark curves* represent the iterative sliding-mode controller and the direct sliding-mode controller, respectively. The direct SMC trajectory exhibits no observable overshoot and smaller oscillations around the reference angle, while the iterative SMC trajectory exhibits nearly 40% overshoot.

desired angle than the iterative SMC, a reduction of around 30%, as the valve configuration used in the direct SMC method allows the pressure required to maintain the desired angle to be held within the actuator.

Thus, barring leakage, the direct SMC is capable of holding constant angles indefinitely without error. The fluc-


FIG. 7. Dynamic response of both controllers following sinusoidal trajectories with frequencies of 0.25 Hz **(a)**, 1 Hz **(b)**, 4 Hz **(c)**, and 6 Hz **(d)**, with the same bending angle amplitude of 34.3°. The *dashed line* is the desired trajectory and the *light* and *dark curves* are the iterative and the direct sliding-mode controllers, respectively.

tuation that can be seen in the direct SMC data is the result of sensor noise. In addition, the direct SMC reaches the desired angle with significantly less overshoot than the iterative SMC. The direct SMC had almost none (less than its steady-state fluctuation), while the iterative SMC demonstrated a 40% overshoot and only settled down after 0.4 s (as opposed to 0.2 s for the direct SMC).

Figure 7 shows the two controllers following four periods of sine waves at an amplitude of 0.6 rad (34.3°) and frequencies ranging from 0.25 to 6 Hz. There is little difference between the performances of the two controllers at less than 1 Hz, because both controllers are faster than the reference signals. However, the direct SMC demonstrates superior performance at higher frequencies, with a 15% higher amplitude and a phase delay of 0.5 rad less than the iterative SMC at 6 Hz. It can be seen that the direct SMC trajectory is closer to the desired trajectory at higher amplitudes, with larger amplitudes and less phase delay than the iterative SMC. In addition, the direct SMC exhibits less vibration than the iterative SMC.

However, at the lowest frequency, the direct SMC trajectory has larger fluctuations. This is because the direct SMC can only either hold position or apply full pressure in either direction. Thus, when the desired position is outside the dead zone but nearby, the SMC will cause the actuator to move rapidly, with limitations in the valve response time causing it to overshoot the desired position slightly, before undergoing damped oscillation around the desired position. During low-frequency signal following, the desired trajectory keeps moving just outside the dead zone, causing this behavior to occur over the entire trajectory. Under these circumstances,
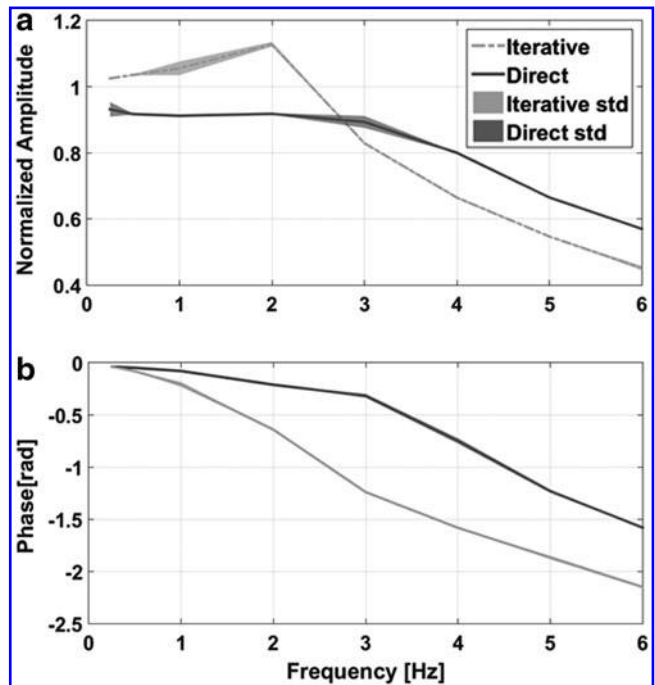
FIG. 8. Closed loop frequency response of both controllers tracking sinusoidal signals over a range of frequencies. The normalized amplitude **(a)** and phase delay **(b)** data indicate that the direct sliding-mode controller offers superior tracking performance with improved phase delay and more uniform amplitude values.
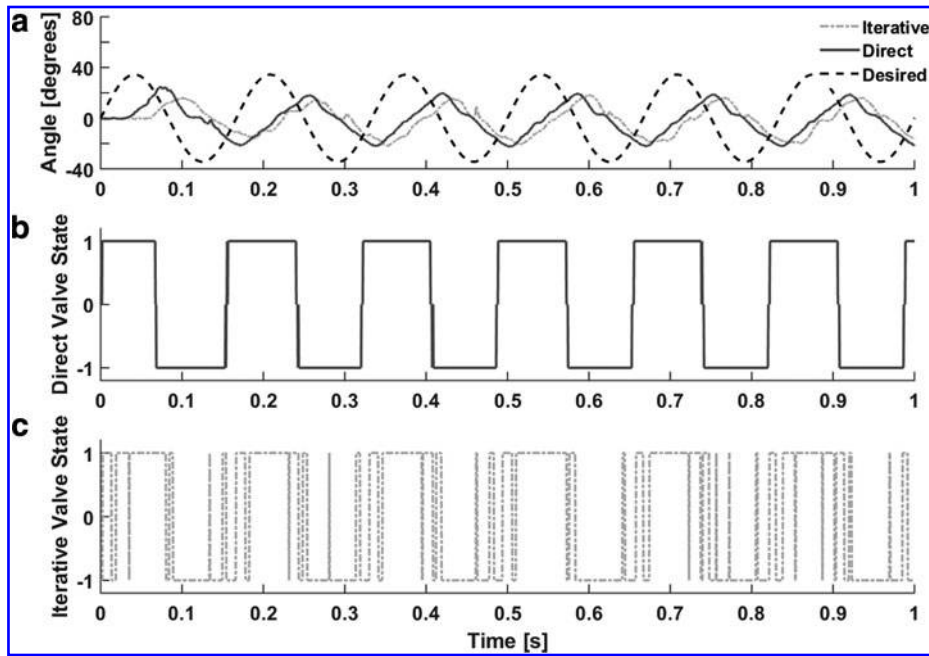
FIG. 9. (a) Iterative and direct SMC system trajectories for 6 Hz sine wave following. The corresponding valve states for the direct (b) and the iterative SMC (c), where 1 represents bending actuation in the positive direction, 0 represents holding (applies only to the direct SMC), and −1 represents bending actuation in the negative direction.

the iterative SMC will change the duty cycle slightly, causing the new average actuator position to increase slightly, resulting in a smoother transition for smaller disturbances.

To demonstrate the performance variation between the two controllers, Figure 8a, b shows the aggregated normalized amplitude and phase delay for each controller at each frequency. These data show that the direct SMC has a much higher bandwidth than the iterative SMC, exhibiting little increase in phase delay as frequency increased, to a maximum of 0.5 rad. The direct SMC also has a higher amplitude at higher frequencies, consistently around 10 percentage points higher, as the amplitude of the iterative SMC drops off steeply. In addition, the differences in standard deviation

between the two controllers show that the direct SMC results in less vibration, as expected.

We have had concerns about the lifetime of valves under this type of rapid actuation. In particular, we have observed that the continuous actuation of the iterative SMC has had a deleterious effect on the valves being used. To investigate this, we recorded the valve states of the controllers as they operated, allowing us to the keep track of how many times each valve was cycled.

First, we did this test for sine wave following at 6 Hz (with amplitude = 0.6 rad, as before), the results of which can be seen in Figure 9a–c. At 6 Hz, the system cannot respond quickly enough to follow the sine waves accurately, and thus
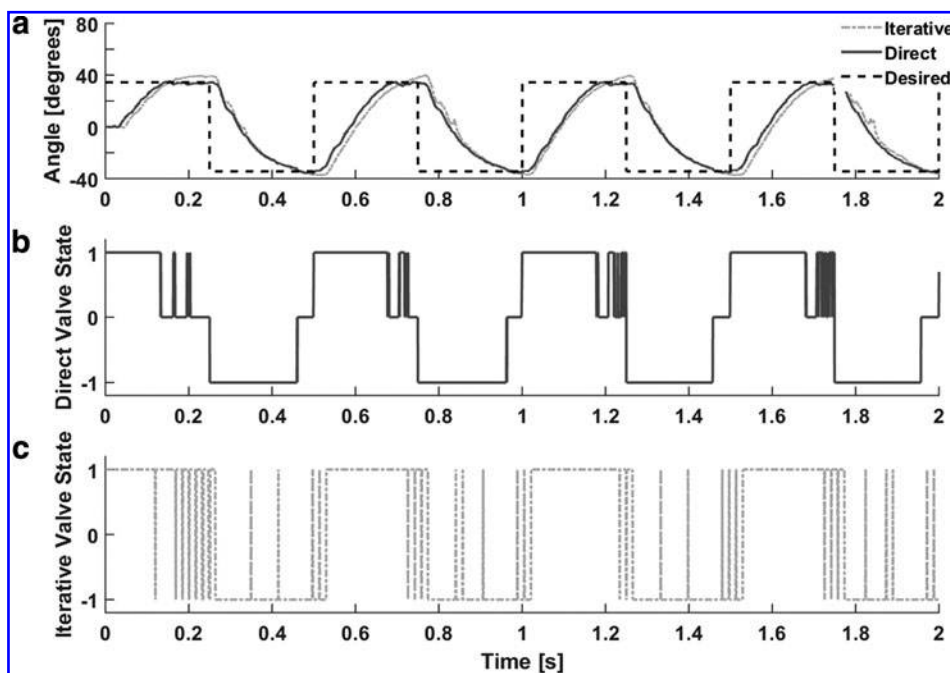
FIG. 10. (a) Iterative and direct SMC system trajectories for 2 Hz *square wave* following. The corresponding valve states for the direct (b) and the iterative SMC (c), where 1 represents bending actuation in the positive direction, 0 represents holding (applies only to the direct SMC), and −1 represents bending actuation in the negative direction.

alternate between full actuation in either direction. We can see from plots (b, c) that the iterative SMC actuates each valve more often for an inferior performance. Over 10 s of constant 6 Hz sine wave following, the direct SMC drives each of its valves a total of 67 times compared to the iterative SMCs 349 times. Thus, under this operation, valves of a system using the direct SMC are likely to last five times as long as those using the iterative SMC.

We also performed the same test when following a 2 Hz square wave with an amplitude of 0.6 Rad (34.3°), which can be seen in Figure 10a–c. This is a slower frequency than the previous test, which allows the system to reach the desired angle and hold. We can see from Figure 10b, c that once the desired angle has been reached, the direct SMC stops actuating each valve, while the iterative SMC must continue to repeatedly switch between the two states to hold position. Over 10 s of tracking a 2 Hz square wave, the direct SMC actuates each valve 26 times, while the iterative SMC actuates each valve 213 times, an increase of over eight times the number of switching commands per valve. This improvement will increase for trajectories that involve maintaining a constant angle for extended periods of time, which the proposed direct SMC can do without any continuous valve actions.

Conclusion

In this article, we discussed our latest developments in pressure-operated soft bending actuation. We modified our Hall effect curvature sensor and actuator chamber cross section to achieve more reliable proprioceptive sensing. We modified our pneumatic circuit to include solenoid valves on the inlet and outlet of each chamber. This allowed us to derive and implement a direct sliding-mode controller algorithm on valve states with the ability to hold the actuator steady without continuous pressurization and depressurization.

We demonstrated the superiority of this controller over our previously developed iterative sliding-mode controller in following static and dynamic trajectories of frequencies ranging from 0.25 to 6 Hz. In addition, we demonstrated a reduction in valve actuations of the direct SMC compared to the iterative SMC, indicating that the former is conducive to longer lifetimes for solenoid valves.

One potential problem with the valving used for the direct SMC approach is it requires two on/off valves for each pressure chamber, and thus requires double the amount of control signals. This was not a problem for a single bidirectional bending segment with two chambers, but would be more of a difficulty for larger systems with more degrees of freedom. In addition, while the valves are relatively small, on a self-contained system the doubling of the required valves could take up a prohibitive amount of space, perhaps outweighing the improvements it provides.

The ability of the direct SMC to follow static trajectories relies on a well-sealed pneumatic system. Any leaks will cause it to drift away from a desired static angle. Once it leaves the dead zone ε, the control system will respond and experience some oscillation before becoming steady again. This behavior results in much larger oscillations than the iterative SMC around a steady state. As our soft robotic snake locomotion requires dynamic trajectories from each module,[22] this will likely not be a problem for that application. On the contrary, for these modules to be used in a soft manipu-lator, the ability to remain steady will likely be useful, requiring the chambers to remain well sealed.

The next step is to adapt this soft actuation module for use in our soft robotic snake. These will be easy to assemble in series to form the body of the snake. The modular nature will allow the snake to be easily repaired and expanded, letting us investigate grasping and redundant locomotion toward a soft mobile manipulator in future work.

Author Disclosure Statement

C.D.O. and S.O. are inventors on a patent application (no. 15/064,872) submitted by WPI that covers soft-body deformation and force sensing. The remaining authors declare that they have no competing interests.

References

1. Lipson H. Challenges and opportunities for design, simulation, and fabrication of soft robots. Soft Robot 2014;1:21–27.
2. She Y, Ji C, Shi H, Su H. Modeling and validation of a novel bending actuator for soft robotics applications. Soft Robot 2016;3:71–81.
3. Hines L, Kirstin P, Metin S. Inflated soft actuators with reversible stable deformations. Adv Mater 2016;28:3690–3696.
4. Waynelovich J, Frey T, Baljon A, Salamon P. Versatile and dexterous soft robotic leg system for untethered operations. Soft Robot 2016;3:64–70.
5. Trimmer BA, Takesian AE, Sweet BM, Rogers CB, Hake DC, Rogers DJ. Caterpillar locomotion: a new model for soft-bodied climbing and burrowing robots. 7th International Symposium on Technology and the Mine Problem. Monterey, CA: Mine Warfare Association 2006;1:1–10.
6. Tolley MT, Shepherd RF, Mosadegh B, Galloway KC, Wehner M, Karpelson M, et al. A resilient, untethered soft robot. Soft Robot 2014;1:213–223.
7. Shepherd RF, Llievski F, Choi W, Morin SA, Stokes AA, Mazzeo AD, et al. Multigait soft robot. Proc Natl Acad Sci U S A 2011;108:20400–20403.
8. Marchese AD, Komorowski K, Onal CD, Rus D. Design and control of a soft and continuously deformable 2d robotic manipulation system. 2014 IEEE International Conference on Robotics and Automation (ICRA). IEEE 2014: 2189–2196.
9. Kapadia AD, Walker ID, Dawson DM. A model-based sliding mode controller for extensible continuum robots. Proceedings of the 9th WSEAS international conference on Signal processing, robotics and automation. World Scientific and Engineering Academy and Society (WSEAS), 2010:113–120.
10. Renda F, Giorelli M, Calisti M, Cianchetti M, Laschi C. Dynamic model of a multibending soft robot arm driven by cables. IEEE Trans Robot 2014;30:1109–1122.
11. Chen G, Pham MT, Redarce T. Sensor-based guidance control of a continuum robot for a semi-autonomous colonoscopy. Robot Auton Syst 2009;57:712–722.

12. Cecilia L, Matteo C, Barbara M, Laura M, Maurizio F, Paolo D. Soft robot arm inspired by the octopus. Adv Robot 2012;26:709–727.

13. Bishop-Moser J, Krishnan G, Kim C, Kota S. Design of soft robotic actuators using fluid-filled fiber-reinforced elastomeric enclosures in parallel combinations. 2012 IEEE/RSJ International Conference on Intelligent Robots and Systems. IEEE 2012:4264–4269.

14. Kim S, Hawkes E, Cho K, Jolda M, Foley J, Wood RJ. Micro artificial muscle fiber using NiTi spring for soft robotics. 2009 IEEE/RSJ International Conference on Intelligent Robots and Systems. IEEE 2009:2228–2234.

15. Polygerinos P, Wang Z, Overvelde JT, Galloway KC, Wood RJ, Bertoldi K, *et al*. Modeling of soft fiber-reinforced bending actuators. IEEE Trans Robot 2015;31: 778–789.

16. Moers AJM, De Volder MFL, Reynaerts D. Integrated high pressure microhydraulic actuation and control for surgical instruments. Biomed Microdevices 2012;14:699–708.

17. Bae J, De Rossi SMM, O'Donnell K, Hendron KL, Awad LN, Teles Dos Santos TR, *et al*. A soft exosuit for patients with stroke: feasibility study with a mobile off-board actuation unit. 2015 IEEE International Conference on Rehabilitation Robotics (ICORR). IEEE 2015:131–138.

18. Menguc Y, Park Y-L, Martinez-Villalpando E, Aubin P, Zisook M, Stirling L, *et al*. Soft wearable motion sensing suit for lower limb biomechanics measurements. Robotics and Automation (ICRA), 2013 IEEE International Conference on. IEEE 2013:5309–5316.

19. Onal CD, Rus D. Autonomous undulatory serpentine locomotion utilizing body dynamics of a fluidic soft robot. Bioinspir Biomim 2013;8:026003.

20. Luo M, Agheli M, Onal CD. Theoretical modeling and experimental analysis of a pressure-operated soft robotic snake. Soft Robot 2014;1:136–146.

21. Ozel S, Skorina EH, Luo M, Tao W, Chen F, Pan Y, *et al*. A composite soft bending actuation module with integrated curvature sensing. 2016 IEEE International Conference on Robotics and Automation (ICRA). IEEE 2016:4963–4968.

22. Luo M, Pan Y, Skorina EH, Tao W, Chen F, Ozel S, *et al*. Slithering towards autonomy: a self-contained soft robotic snake platform with integrated curvature sensing. Bioinspir Biomim 2015;10:055001.

23. Tao W, Skorina EH, Chen F, McInnis J, Luo M, Onal CD. Bioinspired design and fabrication principles of reliable fluidic soft actuation modules. 2015 IEEE International Conference on Robotics and Biomimetics (ROBIO). IEEE 2015:2169–2174.

24. Park Y-L, Chau K, Black RJ, Cutkosky MR. Force sensing robot fingers using embedded fiber Bragg grating sensors and shape deposition manufacturing. Proceedings 2007 IEEE International Conference on Robotics and Automation. IEEE 2007:1510–1516.

25. Xu R, Yurkewich A, Patel RV. Curvature, Torsion, and Force Sensing in Continuum Robots Using Helically-Wrapped FBG Sensors. IEEE Robot Autom Lett 2016;1: 1052–1059.

26. Yi J, Zhu X, Shen L, Sun B, Jiang L. An orthogonal curvature fiber Bragg grating sensor array for shape reconstruction. Life System Modeling and Intelligent Computing. Springer Berlin Heidelberg 2010:25–31.

27. Majidi C, Kramer R, Wood RJ. A non-differential elastomer curvature sensor for softer-than-skin electronics. Smart Mater Struct 2011;20:105017.

28. Kramer RK, Majidi C, Sahai R, Wood RJ. Soft curvature sensors for joint angle proprioception. 2011 IEEE/RSJ International Conference on Intelligent Robots and Systems. IEEE 2011:1919–1926.

29. Kramer RK, Majidi C, Wood RJ. Wearable tactile keypad with stretchable artificial skin. Robotics and Automation (ICRA), 2011 IEEE International Conference on. IEEE 2011:1103–1107.

30. Ozel S, Keskin NA, Khea D, Onal CD. A precise embedded curvature sensor module for soft-bodied robots. Sensor Actuat A Phys 2015;236:349–356.

31. Zhao H, Huang R, Shepherd RF. Curvature control of soft orthotics via low cost solid-state optics. 2016 IEEE International Conference on Robotics and Automation (ICRA). IEEE 2016:4008–4013.

32. Skorina EH, Luo M, Ozel S, Chen F, Tao W, Onal CD. Feedforward augmented sliding mode motion control of antagonistic soft pneumatic actuators. 2015 IEEE International Conference on Robotics and Automation (ICRA). IEEE 2015:2544–2549.

Address correspondence to:
Cagdas D. Onal
Mechanical Engineering Department
Robotics Engineering Program
Worcester Polytechnic Institute
100 Institute Road
Higgins Labs 130
Worcester, MA 01609

E-mail: cdonal@wpi.edu